Journal of Magnetic Resonance 197 (2009) 213–218

Contents lists available at ScienceDirect

Journal of Magnetic Resonance

journal homepage: www.elsevier.com/locate/jmr

T_1 and T_2 effects during radio-frequency pulses in spoiled gradient echo sequences

Nicolas Boulant *

CEA, DSV, I2BM, NeuroSpin, LRMN, Gif sur Yvette 91191, France

ARTICLE INFO

Article history:
Received 19 August 2008
Revised 29 December 2008
Available online 13 January 2009

Keywords:
Magnetic resonance imaging
RF pulses
Relaxation
Spoiled gradient echo sequences

ABSTRACT

Finite pulse durations in diverse pulse schemes lead to the reduction of the magnitude of the magnetization vector due to T_1 and T_2 effects during the radio-frequency pulses. This paper presents an analysis of the steady state signal in the presence of relaxation effects during radio-frequency pulses in MRI spoiled gradient echo sequences. It is shown that minor attenuations of the magnetization vector can have dramatic consequences on the measured signal, and may thus entail a loss in SNR benefits at high static magnetic fields if a careful analysis is not performed. It is emphasized that it is the time-integrated magnetization vector trajectory that matters for these effects and not only the pulse duration. Some experimental results obtained on a phantom at 3 T verify this analysis.

1. Introduction

Radiofrequency (RF) or B_1 inhomogeneity is a major problem in MRI at high field which arises from destructive interferences and dielectric resonance effects [1,2]. For volumes whose dimensions are comparable or larger than the RF wavelength, the gain of the high magnetic fields would be reduced if substantial measures were not taken to counteract that phenomenon. For the last few years, a lot of research has been dedicated to this problem and has given birth to new powerful tools and techniques including shaped pulses [3–8], RF shimming [9–11] and Transmit SENSE [12–15]. Besides RF shimming where it is the transmitted B_1 field itself that one tries to make uniform, but where the region over which it can be done is limited because of the constraints of Maxwell's equations [9,10], other schemes ultimately aim at homogenizing the spin flip angle (FA) and in general require RF irradiations of a few milliseconds or more [3–8,12–15]. In the case of high T_1, low T_2 and small TR values, relaxation effects during RF pulses in standard MRI sequences such as the spoiled gradient echo sequence (SPGE) can no longer be ignored. The purpose of this paper is to demonstrate their impact in these sequences. We first provide via a simplified model a derivation of the steady state signal by examining the transient nutations of the nuclear spins in the presence of relaxation. It is shown that the attenuation of the magnetization vector due to these effects can sometimes have a dramatic impact in the MRI experiment, reaching in some cases a several-fold reduction of signal. The key is to realize that although the attenuation of the magnetization vector due to these effects might be quite small, on the order of one to some percent, it can be comparable to $E_1 = \exp(-TR/T_1)$ in the short TR/T_1 ratio applications, and can therefore play an important role. Second, we report a 3D SPGE experiment on a phantom at 3 T to validate the analysis. We finally discuss the results and their implications. Note that within the context of MRI, relaxation effects during RF pulses have already been studied in magnetization transfer experiments [16], where long and off-resonance pulses are usually applied to saturate the macromolecular protons, and to determine potential degradations of frequency profiles of selective pulses [17]. This will not be our concern here and we shall rather focus merely on the impact of self-relaxation (as opposed to cross-relaxation) effects for the protons in bulk water only, whether the pulses are meant to be selective or not.

2. Theory

2.1. Simplified dynamics during the RF pulse

We take the simplest case of a constant amplitude and on-resonance pulse along the x-axis with an initial state of the Bloch vector in the y–z plane. The general solution for off-resonance irradiation can be found in [18]. In the conditions mentioned above, the magnetization vector dynamics are described by the phenomenological Bloch equation [18], which in the frame rotating at the spin resonance frequency is:

$$\begin{aligned} \frac{dM_y}{dt} &= -R_2 M_y + \omega_1 M_z \\ \frac{dM_z}{dt} &= -\omega_1 M_y - R_1 (M_z - M_0) \end{aligned} \tag{1}$$

where $[M_x M_y M_z]^{\mathrm{T}}$ is the Bloch magnetization vector (M_x remains zero given the assumptions mentioned above), ω_1 is the RF nutation

* Fax: +33 169087855.
E-mail address: nicolas.boulant@cea.fr

1090-7807/$ - see front matter © 2009 Elsevier Inc. All rights reserved.
doi:10.1016/j.jmr.2008.12.023

angular frequency (in rad/s), M_0 is the macroscopic magnetization at thermal equilibrium, $R_1 = 1/T_1$ and $R_2 = 1/T_2$ are the relaxation rates. Written in matrix form, the former set of equations can be recast as:

$$\frac{d}{dt}\begin{pmatrix} M_y \\ M_z \end{pmatrix} = \underbrace{\begin{pmatrix} -R_2 & \omega_1 \\ -\omega_1 & -R_1 \end{pmatrix}}_{A}\begin{pmatrix} M_y \\ M_z \end{pmatrix} + \begin{pmatrix} 0 \\ R_1 M_0 \end{pmatrix} \tag{2}$$

whose solution for the initial state $\mathbf{M(0)} = [0\, M_y(0) M_z(0)]^{\mathrm{T}}$ is $M_x = 0$ and

$$\begin{pmatrix} M_y \\ M_z \end{pmatrix}(t) = e^{At}\begin{pmatrix} M_y(0) \\ M_z(0) \end{pmatrix} + (\mathbf{Id} - e^{At})\begin{pmatrix} M_{y,ss} \\ M_{z,ss} \end{pmatrix} \tag{3}$$

where $\mathbf{Id}$ is the 2 by 2 identity matrix while $M_{y,ss}$ and $M_{z,ss}$ are the steady state values under constant RF irradiation along the y- and z-axis, respectively. These steady state values are given by [19]:

$$M_{y,ss} = M_0\frac{\omega_1 R_1}{R_1R_2 + \omega_1^2} \quad \text{and} \quad M_{z,ss} = M_0\frac{R_1R_2}{R_1R_2 + \omega_1^2}.$$

The solution therefore consists of a first term, linear with respect to the initial magnetization vector $\mathbf{M(0)}$, and a second term which depends on the relaxation terms, the magnetization at thermal equilibrium and the RF field amplitude. In most cases, the RF nutation frequency will be such that $\omega_1 \gg R_1, R_2$ so that for pulses whose durations are short compared to T_1 and T_2, the second term on the right hand side of Eq. (3) can be neglected. Assuming $M_y(0)^2 + M_z(0)^2 = 1$, to first order in $\delta = (R_2 - R_1)/2\omega_1$ the final form of the magnetization vector is

$$\begin{pmatrix} M_y \\ M_z \end{pmatrix}(t) \approx \exp(-R_{Av}t) \times \begin{pmatrix} M_y(0)\cos(\Omega_1 t) - M_y(0)\delta\sin(\Omega_1 t) + M_z(0)\sin(\Omega_1 t) \\ M_z(0)\cos(\Omega_1 t) + M_z(0)\delta\sin(\Omega_1 t) - M_y(0)\sin(\Omega_1 t) \end{pmatrix} \tag{4}$$

where $R_{Av} = (R_1 + R_2)/2$ is the average relaxation rate, and $\Omega_1 = \omega_1(1 - \delta^2)^{1/2}$ is the effective RF nutation frequency. The norm of the vector at the end of the pulse of duration T is

$$n(T) \approx \exp(-R_{Av}T)\Big[1 + \frac{\delta}{2}\sin(2\Omega_1 T)(M_z(0)^2 - M_y(0)^2) - 2\delta M_z(0)M_y(0)\sin^2(\Omega_1 T)\Big]. \tag{5}$$

As the RF field amplitude increases, δ decreases. As a result, depending on $\mathbf{M(0)}$, and if $\Omega_1 T < \pi/2$, the second term on the right hand side of Eq. (5) also increases if $M_z(0) = 0$, and decreases if $M_y(0) = 0$. Several things can be learnt from these results. First, for a given square pulse duration, the smaller ω_1 is, there is less (more) attenuation if the initial magnetization vector starts along the $z(y)$ axis. This just illustrates the fact that when T_2 is shorter than T_1, the more magnetization there is in the transverse plane, the more the total magnetization vector shrinks. Second, the higher the RF field, the better n can be approximated by $\exp[-(R_2 + R_1)T/2]$. This means that when the RF field is sufficiently strong, it mixes the longitudinal and transverse components equally so that the Bloch vector decays at a rate which is the average of R_1 and R_2. For very short pulses, the attenuation is negligible. However, when trying to homogenize the FA by using longer shaped pulses and complicated trajectories on the Bloch sphere, a few percent attenuations can be achieved. Finally, one can see from Eq. (4) that the rotation part of the transformation is barely affected by relaxation. To zeroth order in $(R_2 - R_1)/2\omega_1$ the rotation angle is as if no relaxation was present, i.e. equal to $\omega_1 t$ (a result consistent with [20]). Despite the particular conditions for which the result above was derived, we have found this simple model to be quite useful to provide insight and first estimation of the attenuation of the magnetization vector for more complicated pulse shapes, when the initial state is along the z axis. If an RF pulse $\omega_1(t)$ of length T, with a constant phase in the rotating frame, is such that $(R_2 - R_1)/2\omega_1 \ll 1$ at all times, then because the attenuation does not depend on $\omega_1(t)$ to zeroth order, the value of n is, to a good approximation, given by $\exp[-(R_2 + R_1)T/2]$. Hence in this regime, it uniquely depends on the pulse duration T. In many cases however, the variation of $\omega_1(t)$ is not always such that the above condition is fulfilled so that n depends on ω_1 and hence on the trajectory taken by the magnetization vector. This analysis of course strictly applies to on-resonance pulses with constant phase. When modulating the phase $\phi(t)$ of the RF pulse in time, a three-dimensional Bloch vector description is necessary [18]. Note however, that when the pulse shape is approximated as a series of steps with discretization time Δt, and still in the frame rotating at the spin resonance frequency, Bloch equation at time $t = k\Delta t$ (k is an integer) reads

$$\frac{d}{dt}\begin{pmatrix} M_x \\ M_y \\ M_z \end{pmatrix} = \begin{pmatrix} -R_2 & 0 & \omega_{1,k}\sin\phi_k \\ 0 & -R_2 & -\omega_{1,k}\cos\phi_k \\ -\omega_{1,k}\sin\phi_k & \omega_{1,k}\cos\phi_k & -R_1 \end{pmatrix}\begin{pmatrix} M_x \\ M_y \\ M_z \end{pmatrix} + \begin{pmatrix} 0 \\ 0 \\ R_1M_0 \end{pmatrix} \tag{6}$$

where $\omega_{1,k}$ and ϕ_k are the RF nutation frequency and the phase, respectively, at the same instant $k\Delta t$. By changing basis, i.e. via a ϕ_k rotation about z, one obtains a system of equations similar to Eq. (4) which can be solved to yield $M((k + 1)\Delta t)$. In that frame, the magnetization vector can be decomposed with a z-longitudinal component, a transverse component along the RF direction and another transverse component perpendicular to the other two. The first and third components evolve as described above, while the second one decays with the rate R_2. At the end of the pulse, the attenuation of the magnetization vector will result from the combined action of the relaxation and the rotation parts.

2.2. BIR-4 and strongly modulating pulse simulations

To illustrate the previous discussion, we have simulated the spins' dynamics by integrating the Bloch equation including the relaxation parameters of gray matter measured at 7 T [21] under the action of a BIR-4 [8,22] and a strongly modulating pulse (SMP) [6]. The BIR-4 pulse was a tanh/tan pulse with duration 5 ms, frequency excursion 7 kHz, parameters $\lambda = 10$ and $\tan\beta = 10$ [22], while the SMP pulse lasted 3.894 ms and was designed to homogenize the FA over a human brain at 7 T. The target FA in each case was 30°. In each simulation, the Bloch vector was starting along the *z-axis.* We varied the peak B_1 amplitude and calculated the corresponding FA and norm n of the magnetization vector. Fig. 1a and b shows the former and latter quantities, respectively. In spite of relaxation, both pulses meet their expected FA homogenizing performance. On the other hand, there is a significant variation of n with respect to the peak B_1 amplitude and hence on the magnetization vector trajectory, unless, for the BIR-4 pulse, the RF amplitude is above a certain threshold (far above R_2 and R_1). Hence despite the efforts to homogenize the FA with respect to the RF amplitude, some inhomogeneity in n may still remain.

2.3. Repetition of the same pulse with transverse spoiling

When repeating the same RF pulse every TR seconds, and ignoring the second term in Eq. (3), the steady state transverse magnetization in a SPGE sequence becomes proportional to

$$S_{Relax}(n,\theta) \propto \frac{1 - E_1}{1 - E_1 n\cos\theta} n\sin\theta \tag{7}$$

where $E_1 = \exp(-TR/T_1)$ and θ is the FA [23]. As mentioned above, n is the length of the magnetization vector after the RF pulse normalized by the one before it. For pulse durations on the order of hun-

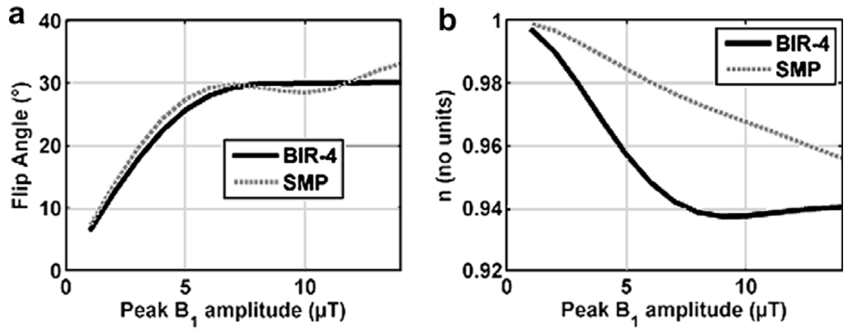

Fig. 1. Flip angle (inset a) and magnitude n (inset b) of the magnetization vector for a 30° BIR-4 and a 30° strongly modulating pulse (SMP). The BIR-4 pulse was a tanh/tan pulse with duration 5 ms, frequency excursion of 7 kHz, parameters $\lambda = 10$ and $\tan\beta = 10$ [22], while the SMP pulse was 3.894 ms long. In each simulation, the FA and attenuation of the magnetization vector were calculated with respect to the peak B_1 amplitude, by integrating the Bloch equation including the relaxation parameters of gray matter measured at 7 T [21]. Inset a shows the ability for both pulses to homogenize the FA while inset b shows a clear dependence of n with respect to the peak B_1 amplitude. Although the FA might be relatively uniform over some range of B_1 values, some inhomogeneity in n and hence of the measured signal may still remain.

dreds of μs, n is usually very close to 1 and one recovers in this limit the usual signal formula $S_{Relax}(n = 1,\theta)$ whose maximum is reached at the Ernst angle $\theta_E = a\cos(E_1)$ [23]. The true Ernst angle $\theta_{E,\ Relax}$ otherwise is $a\cos(nE_1)$. Calculating the ratio $S_{Relax}(n = 1,\theta)$ over $S_{Relax}(n \neq 1,\theta)$ at θ_E yields $S_{Relax}(n = 1,\theta_E)/S_{Relax}(n \neq 1,\theta_E) \approx 1 + \varepsilon/(1 - E_1^2)$ for small ε, where $\varepsilon = 1 - n$, which can be further simplified to first order in TR/T_1 as

$$S_{Relax}(n = 1, \theta_E)/S_{Relax}(n \neq 1, \theta_E) \approx 1 + \epsilon T_1/2TR. \quad (8)$$

Taking 1900 ms as the T_1 value for gray matter (GM) at 7 T [21], TR = 100 ms, and $\varepsilon = 0.01$ (obtained for instance when $n \approx \exp(-R_{Av}T)$ with T = 1 ms, R_2 = 1/0.051 s^{-1} and R_1 = 1/1.9 s^{-1}) yields a ratio of nearly 1.1, i.e. already a 9% attenuation of the signal. Shorter TR values increase the signal loss. For TR = 7.1 ms and $\varepsilon = 0.01$, the signal drops by a factor of 2.34, i.e. the theoretical gain of polarization at thermal equilibrium obtained when moving from a 3 to a 7 T field strength. Note that this does not challenge the quasi-linear gain in SNR with the external field: spin polarization combined with Faraday's law still imply for the signal a quadratic dependence on B_0, while the noise is still roughly proportional to B_0 at high fields [23]. Caution is simply advised regarding the RF conditions in which SNR measurements are carried out.

A plot of $S_{Relax}(n,\theta)$ is provided in Fig. 2 for several values of n, and for two different TR values. The above signal reduction was calculated at the Ernst angle because of the mathematical simplicity of the final result (Eq. (8)). At other flip angles, as can be seen in Fig. 2, the loss can also be substantial. Further inspection of Eq. (8) also indicates a possible loss of contrast between different tissues, depending on their respective T_1 and ε values. Finally, note that provided that $\omega_1 \gg \gamma\Delta B_0$, where $\gamma\Delta B_0$ is the spread of resonance frequencies within a voxel and γ is the gyromagnetic ratio, it is truly T_2 that should be taken into account above and not T_2^* [18,19].

3. Experiment

3.1. SPGE measurements

Our measurements were performed on a Siemens 3 T Trio scanner (Siemens Medical Solutions, Erlangen, Germany) with a body coil used for transmission and a 12-channel head coil for reception. The main goal of the experiment was to confirm Eq. (7). The gradient amplitudes and slew rates available were 40 mT/m and 200 T/m/s, respectively. Our SPGE sequences were implemented on a liquid phantom made of 2 L of distilled water that we prepared with a concentration of 5 mM of $CuSO_4$ and 0.23 mM of Sinerem (Guerbet, Aulnay-sous-Bois, France). To verify Eq. (7), we carried out two series of scans with parameters TR/TE = 30/4 ms, resolution = 3.3 × 3.3 × 3 mm^3, matrix size of 64 × 64 × 64. In the first series, we varied the FA from 4° to 96° in steps of 4° using a 300 μs square pulse, while we used a 3 ms square pulse for the second one, thereby ensuring a duty cycle not larger than 10%. In the second series however, since

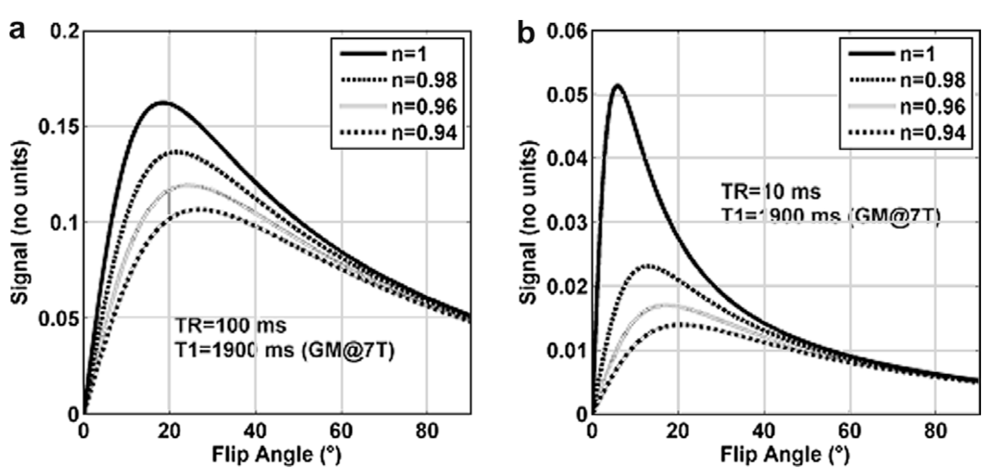

Fig. 2. Theoretical plots of the steady state signal (see Eq. (7)) for different values of n, TR = 100 ms (inset a) and TR = 10 ms (inset b), and for T_1 = 1900 ms (gray matter at 7 T). On both insets, one can see that the smaller n is, the larger the drop of signal is (especially around the Ernst angle). The relative drop is amplified as TR gets smaller and $\theta_{E,Relax}$ increases as n decreases.

$S_{Relax}(\theta)$ is 2π periodic, we varied the FA from 364° up to 456° still in steps of 4°, to fulfill the condition $(R_2 - R_1)/2\omega_1 \ll 1$ and have n quasi-independent on the flip angle. Although one would not employ such pulses in real conditions, we stress that they were used to merely obtain a few percent attenuation of the magnetization vector in an easily controllable manner. What matters is the value of n, not how it is obtained, and the fact that typical shaped RF pulses can lead to comparable attenuations (see Fig. 1b). No magnetic field gradients were applied during RF pulsing.

3.2. Flip angle measurements

To calculate n and compare the experimental results with the theory, knowledge of the FA, T_1 and T_2 is required. Because the FA is inhomogeneous over the sample, we used the modified actual flip angle imaging (MAFI) sequence reported in [24,30] to measure the FA at a reference voltage corresponding to a prescribed FA of $\pi/3$. The sequence yielded a spatially dependent FA_{ref} for that particular voltage. To deduce the FA at other voltages, we performed a linearity check measurement by taping a small wire loop on the phantom, connecting it to an oscilloscope and measuring the induced voltage in the loop versus the voltage entered on the console of the scanner, thus providing a look-up table for the voltages used and the FA implemented. Due to the uncertainty in the initial measurement of the absolute FA of reference, we multiplied FA_{ref} by a fitting parameter α to yield the true FA. The sequence parameters we used for the MAFI sequence were TR_1 = 20 ms and TR_2 = 60 ms (same resolution and matrix size as above). B_0 maps were obtained through fits of the phase evolution monitored using two additional echoes in TR_1 ($TE_{1,2,3}$ = 7, 8.4 and 10 ms) and to verify quasi-resonance. We then looked at the data (image intensity and FA) in a voxel where this condition was met and where the FA excursion roughly was close to the prescribed range of values. We normalized all the data by a second fitting parameter to compensate for the spin density, the reception sensitivity, T_2^* decay during echo acquisition and other possible factors due to the electronics chain, and to compare the data with Eq. (7). The parameter fit was done by using the simplex search method that the MATLAB software provides (The MathWorks, Natick, MA).

3.3. T_1 and T_2 measurements

We measured T_1 and T_2 using an SPGE sequence with an inversion preparation for the former (TI = 30–270 ms in steps of 40 ms, FA = 20° and TR = 400 ms), and a spin–echo sequence for the latter (17 echoes, TE = 6.6 to 112.2 ms in steps of 6.6 ms, TR = 3 s). Knowledge of T_1, T_2 and ω_1 thus allowed the computation of n. In all experiments, we used an apodization filter to reduce Gibbs ringing artefact due to the small image matrix size. The RF pulses used in the MAFI and T_1 measurement experiments were 100 μs long (besides the adiabatic inversion, but which was repeated every 400 ms), thereby leading to a negligible attenuation of the magnetization vector ($n \approx 0.999$). As a result, relaxation during these RF pulses did not alter the result of these measurements. The T_2 measurement on the other hand was biased because of RF inhomogeneity and because the value returned by the scanner was based on a fit assuming instantaneous π pulses (they were in fact 3.84 ms long). Thus an RF field was applied for more than half the time of the echo spacing. The returned value therefore was likely to be overestimated. Hence the relaxation parameter T_2 was also included in the final fit, using the result of the measurement as an initial guess.

4. Results

For the selected voxel (not shown), B_1, B_0, T_1 and T_2 were measured to be 57 nT/V, 1.83 Hz (in the frame rotating at the carrier frequency), 214.4 ms and 53.0 ms, respectively. The fit returned a corrected value of T_2 equal to 35.4 ms, in addition to a correction factor α equal to 0.961 implying a 4% error in the initial FA measurement. With this information, we calculated $n \approx 0.995$ for the 300 μs pulse and $n \approx 0.952$ for the 3 ms one. The B_1 and B_0 maps are given for a central slice of the phantom in Fig. 3.

The normalized experimental signals versus the flip angle are provided in Fig. 4 along with the linearity check measurement results of the amplifier in the inset. The RMS error between experiment and theory is 1.2% for the 300 μs pulse data and 2.8% for the 3 ms one, indicating very good agreement between the two. We found that the linearity was within the specifications of the amplifier, with a deviation of less than 5% over the full range of voltages tested (0–450 V). Nevertheless, without this measurement and the resulting corrections due to small non-linearities, the agreement between theory and experiment was poorer, with a noticeable mismatch between the locations of the maxima of the different curves. The T_1 value of the phantom being relatively low, here the signal drop was still moderate with a 15% loss of signal at the Ernst angle.

5. Discussion and conclusions

5.1. Potential loss of signal

In this paper, we have established both theoretically and experimentally the importance of relaxation effects during RF pulses in SPGE experiments, depending on the parameters of the sequence

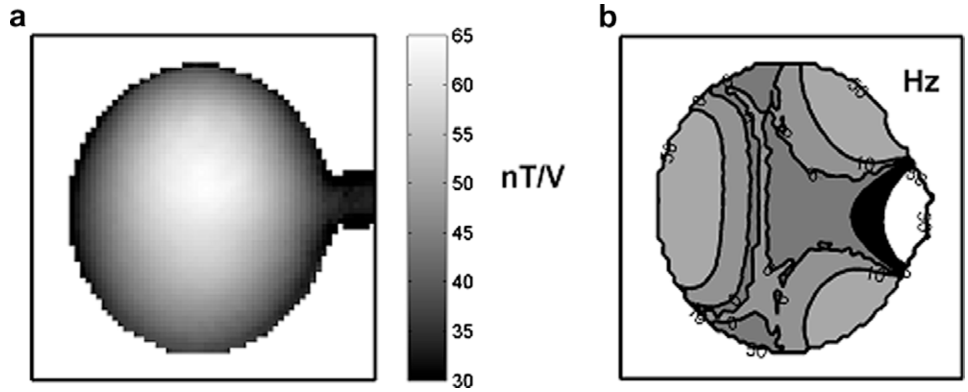

Fig. 3. Measured B_1 and B_0 maps on a central slice of the phantom obtained using the MAFI sequence. (Inset a) B_1 map in nT/V. (Inset b) Contour plot of B_0 in Hz.

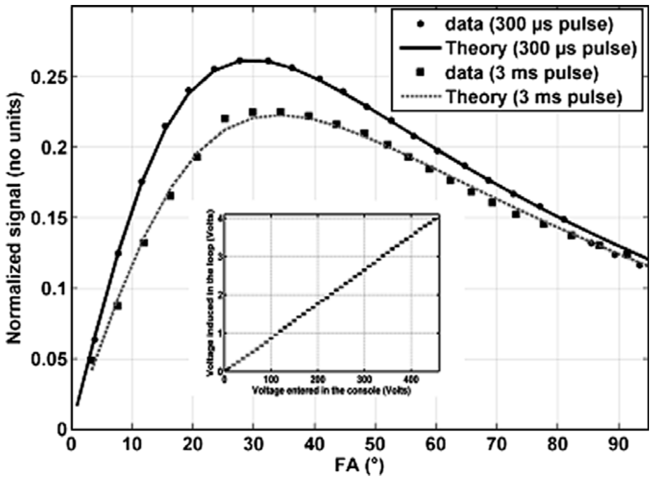

Fig. 4. Normalized signal versus the flip angle for the two different pulse durations: theory and experiment. For the 3 ms pulse data, the FA displayed in the figure is the true one minus 360°. The error bars are not shown for the sake of clarity and are on the order of the size of the symbols. For these scans we had $TR = 30$ ms, $T_1 = 214.4$ ms and $T_2 = 35.4$ ms. (Inset) Voltage induced in the loop versus the voltage entered on the console. The linearity was within the specifications of the amplifier with a deviation of less than 5% over the full range.

and the particular pulse conditions. Although our analysis was done for that MRI sequence only, it is clear that these effects can also play an important role in other sequences. In our data, the signal drop at the Ernst angle was still moderate because of the relatively small T_1 of our phantom. The T_2 value however was somewhat close to the ones reported at 7 T for GM and white matter (WM) [21]. In the same conditions, the T_1 value at that field strength for the former tissue would yield a loss of signal six times larger. Recalling Eq. (8), the loss of signal at the Ernst angle increases with T_1 and ε (and therefore R_2 since the attenuation of the magnetization vector is normally dominated by T_2), and thus with the external field strength [25,26]. It can however, be made small either by taking TR large or by using very short pulses. The former case obviously poses problems for the acquisition of high-resolution in-vivo images, while the latter case adds serious constraints when trying to counteract the RF inhomogeneity problem at high fields. To be more exact, it is not the duration of the pulse itself but the combined action of the relaxation and rotation parts of the dynamics of the magnetization vector during the RF pulse that matters to assess the importance of this effect. If the magnetization vector stays close to the z-axis, for instance when using small FA slice-selective sinc pulses, then ε can be kept small and short TR values can be used without losing too much signal. On the other hand, pulses for instance such as STABLE [5], strongly modulating [6] and BIR-4 pulses [8,22], should be used with caution if the repetition time is short.

5.2. Attenuation of the magnetization vector as a source of signal inhomogeneity

In mathematical control theory, it can be shown that a spin ensemble in MRI is point ensemble controllable if the dynamics obey the Bloch equation without relaxation [27]. This means that an ensemble of spins all starting from the z-axis can be steered to a ball of arbitrary small radius centered on any desired state, in spite of large dispersions in parameters such as the RF power or the Larmor frequency within the ensemble. Of course, doing so would require too large powers and pulse durations to be implemented in in vivo MRI. However, it suggests that the result in [27] does not hold anymore when relaxation is present because the mathematical structure is fundamentally different. If it was indeed the case, it would mean that whatever scheme one may come up with to homogenize the FA with a RF transmission profile constant over time, an intrinsic inhomogeneity would subsist through the non-uniformity of the magnitude of the magnetization vector. The extent to which it could be counteracted remains to be investigated. Parallel transmission schemes provide the degrees of freedom to counteract that phenomenon since the RF transmission profile of the array can vary depending on the relative phases and amplitudes of the respective signals sent to the different coils. Tackling directly this problem of course would come at the expense of great additional complexity in the design of the pulses. Shortening the length of the pulse could on the other hand mitigate this effect indirectly, but at the risk of increasing B_1 and hence the specific absorption rate.

As shown in Fig. 1b, different RF amplitudes lead to different magnetization vector trajectories and as a result, possibly to different attenuations. This however, can sometimes be an advantage. If the FA and n were uniform over a volume of interest, the image intensity would still be inhomogeneous due to the reception profile of the coil. On the other hand, if a transceiver coil is used and if the high transmitted B_1 region coincides with the high reception sensitivity region, then n, if smaller in that region (Fig. 1b), slightly compensates for the reception profile and makes the overall signal of a given tissue more uniform.

5.3. Impact of magnetization transfer in biological tissues

Magnetization transfer between the protons of bulk water and the ones contained in macromolecules in biological tissue certainly plays a major role also when pulsing at high, or even moderate, powers for a few ms with a short repetition time TR [16,28,29]. Pulsing at resonance increases the saturation of the bound protons and makes the effect even more important. In a lot of biological tissues, this phenomenon should therefore be taken into account for a correct and quantitative analysis of the MRI signal [28,29]. With the type of liquid phantom we used in this work, the goal was to isolate the impact of self-relaxation effects, as opposed to cross-relaxation effects, during RF pulses.

To conclude, this paper emphasizes the importance of relaxation effects during RF pulses in SPGE experiments. The image intensity for a given tissue does not only depend on the FA but also on the length of the magnetization vector, which itself depends on its trajectory over time. The significance of these effects increases with the T_1/TR ratio and with R_2, and, as a result increases with static magnetic field strength. It definitely requires careful consideration when designing B_1 and/or B_0 pulse compensation schemes of a few milliseconds or more.

Acknowledgments

This work was funded by the Iseult/Inumac French–German project. We thank B. Marty for preparing the sample. We also thank A. Amadon and P. Cappellaro for valuable discussions. Finally, we thank the reviewer for pointing Ref. [20] to us.

References

[1] P.F. Van de Moortele, C. Akgun, G. Adriany, S. Moeller, J. Ritter, C.M. Collins, M.B. Smith, J.T. Vaughan, K. Ugurbil, B_1 destructive interferences and spatial phase patterns at 7 T with a head transceiver array coil, Magn. Reson. Med. 54 (2005) 1503–1518.
[2] Q.X. Yang, J. Wang, X. Zhang, C.M. Collins, M.B. Smith, H. Liu, X.H. Zhu, J.T. Vaughan, K. Ugurbil, W. Chen, Analysis of wave behavior in lossy dielectric samples at high field, Magn. Reson. Med. 47 (2002) 982–989.
[3] S. Saekho, F.E. Boada, D.C. Noll, V.A. Stenger, Small tip angle three-dimensional tailored radiofrequency slab-select pulse for reduced B_1 inhomogeneity at 3 T, Magn. Reson. Med. 53 (2005) 479–484.

[4] S. Saekho, C.-Y. Yip, D.C. Noll, F.E. Boada, V.A. Stenger, Fast-kz three-dimensional tailored radiofrequency pulse for reduced B1 inhomogeneity, Magn. Reson. Med. 55 (2006) 719–724.
[5] P. Balchandani, J. Pauly, D. Spielman, Slice-selective tunable-flip adiabatic low peak-power excitation (STABLE) Pulse, in: Proceedings of the 16th Annual Meeting of the ISMRM, Toronto, CA, 2008, p. 225.
[6] N. Boulant, D. LeBihan, A. Amadon, Strongly modulating pulses for counteracting RF inhomogeneity at high fields, Magn. Reson. Med. 60 (2008) 701–708.
[7] N. Boulant, D. Le Bihan, A. Amadon, Strongly modulating pulses: a new method for counteracting RF inhomogeneity at high fields, in: Proceedings of the 16th Annual Meeting of the ISMRM, Toronto, 2008, p. 232.
[8] R.S. Staewen, A.J. Johnson, B.D. Ross, T. Parrish, H. Merkle, M. Garwood, 3-D flash imaging using a single surface coil and a new adiabatic pulse, BIR-4, Invest. Radiol. 25 (1990) 559–567.
[9] W. Mao, M.B. Smith, C.M. Collins, Exploring the limits of RF-shimming for high-field MRI of the human head, Magn. Reson. Med. 56 (2006) 918–922.
[10] C.M. Collins, Z. Wang, W. Mao, J. Fang, W. Liu, M.B. Smith, Array-optimized composite pulse for excellent whole-brain homogeneity in high-field MRI, Magn. Reson. Med. 57 (2007) 470–474.
[11] T. Vaughan, L. DelaBarre, C. Snyder, J. Tian, C. Akgun, D. Shrivastava, W. Liu, C. Olson, G. Adriany, J. Strupp, P. Andersen, A. Gopinath, P.F. Van de Moortele, M. Garwood, K. Ugurbil, 9.4 T human MRI: preliminary results, Magn. Reson. Med. 56 (2006) 1274–1282.
[12] U. Katscher, P. Bornert, C. Leussler, J.S. van den Brink, Transmit SENSE, Magn. Reson. Med. 49 (2003) 144–150.
[13] Y. Zhu, Parallel excitation with an array of transmit coils, Magn. Reson. Med. 51 (2004) 775–784.
[14] W. Grissom, C.-Y. Yip, Z. Zhang, A. Stenger, J.A. Fessler, D.C. Noll, Spatial domain method for the design of RF pulses in multicoil parallel excitation, Magn. Reson. Med. 56 (2006) 620–629.
[15] P. Ullmann, S. Junge, M. Wick, F. Seifert, W. Ruhm, J. Hennig, Experimental analysis of parallel excitation using dedicated coil setups and simultaneous RF-transmission on multiple channels, Magn. Reson. Med. 54 (2005) 994–1001.
[16] S.D. Wolff, J. Eng, R.S. Balaban, Magnetization transfer contrast: method for improving contrast in gradient-recalled-echo images, Radiology 179 (1991) 133–137.
[17] R.A. de Graaf, In Vivo NMR Spectroscopy, Principles and Techniques, Wiley and Sons, New York, 1998.
[18] H.C. Torrey, Transient nutations in nuclear magnetic resonance, Phys. Rev. 76 (1949) 1059–1068.
[19] A. Abragam, Principles of Nuclear Magnetism, University Press, Oxford, 2002.
[20] P. Le Roux, Simplified model and stabilization of SSFP sequences, J. Magn. Reson. 163 (2003) 23–37.
[21] J. Pfeuffer, H. Merkle, M. Beyerlein, T. Steudel, N.K. Logothetis, Anatomical and functional MR imaging in the macaque monkey using a vertical large-bore 7 T setup, Magn. Reson. Imaging 10 (2004) 1343–1359.
[22] M.A. Bernstein, K.F. King, X.J. Zhou, Handbook of MRI Pulse Sequences, Elsevier Academic Press, London, 2004.
[23] E.M. Haacke, R.W. Brown, M.R. Thompson, R. Venkatesan, Magnetic Resonance Imaging, Physical Principles and Sequence Design, Wiley and Sons, New York, 1999.
[24] A. Amadon, N. Boulant, in: Proceedings of the 16th Annual Meeting of the ISMRM, Toronto, 2008, p. 1248.
[25] P.A. Bottomley, T.H. Foster, R.E. Argsersinger, L.M. Pfeifer, A review of normal tissue hydrogen NMR relaxation times and relaxation mechanisms from 1 to 100 MHz: dependence on tissue type, NMR frequency, temperature, species, excision, and age, Med. Phys. 11 (1984) 425–448.
[26] H.W. Fischer, P.A. Rinck, Y.V. Haverbeke, R.N. Muller, Nuclear relaxation of human gray and white matter: analysis of field dependence and implications for MRI, Magn. Reson. Med. 16 (1990) 317–334.
[27] S. Li Jr., N. Khaneja, Control of inhomogeneous quantum ensembles, Phys. Rev. A 73 (2006) 030302.
[28] G.B. Pike, Pulsed magnetization transfer contrast in gradient echo imaging: a two-pool analytic description of signal response, Magn. Reson. Med. 36 (1996) 95–103.
[29] J.G. Sled, G.B. Pike, Quantitative imaging of magnetization transfer exchange and relaxation properties in vivo using MRI, Magn. Reson. Med. 46 (2001) 923–931.
[30] V.L. Yarnykh, Actual flip-angle imaging in the pulsed steady state: a method for rapid three-dimensional mapping of the transmitted radiofrequency field, Magn. Reson. Med. 57 (2007) 192–200.